Journal of Power Sources 194 (2009) 520–525

Contents lists available at ScienceDirect

Journal of Power Sources

journal homepage: www.elsevier.com/locate/jpowsour

Fabrication of single-walled carbon nanotube/tin nanoparticle composites by electrochemical reduction combined with vacuum filtration and hybrid co-filtration for high-performance lithium battery electrodes

Jae Hyun Lee[a,b], Byung-Seon Kong[a], Seung Bo Yang[a], Hee-Tae Jung[a,*]

[a] Department of Chemical and Biomolecular Engineering, Korea Advanced Institute of Science and Technology (KAIST), 335 Gwahangno, Yuseong-gu, Daejeon 305-701, Republic of Korea
[b] Research Park, LG Chem, Ltd., 118 Moonjiro, Yuseong-gu, Daejeon 305-738, Republic of Korea

ARTICLE INFO

Article history:
Received 26 February 2009
Received in revised form 8 April 2009
Accepted 14 April 2009
Available online 3 May 2009

Keywords:
Lithium battery
Carbon nanotubes
Tin nanoparticle
Vacuum filtration
Nanocomposite

ABSTRACT

Hybrids consisting of single-walled carbon nanotubes (SWNTs) and tin nanoparticles are prepared on substrates as anode materials for lithium-ion batteries via two different techniques: (i) hybrid co-filtration by simultaneous vacuum filtration of SWNT/tin nanoparticle hybrid solutions and (ii) a combined technique comprised of vacuum filtration and electrochemical reduction. The resulting hybrid composites are of uniform thickness and consist of a homogeneous dispersion of tin nanoparticles in a SWNT network. In the hybrid films, the tin nanoparticles and SWNTs are in close contact with each other and the substrate. The hybrid films exhibit extended cycle life (capacity retention of 80% at 50th cycle), high power characteristics up to 1.75 mA cm^{-2}, high electrode density up to 5 mg cm^{-2}, and enhanced reversible capacities (535 mAh g^{-1} for composite electrode at 50th cycle) because the aggregation of tin nanoparticles is prevented.

1. Introduction

Carbon nanotube (CNT)/tin nanoparticle composites have attracted considerable attention in recent years due to their enhanced stabilities and reversible capacities as anode materials in lithium-ion batteries [1–7]. Conventional lithium-metal alloys, for example, ones with tin, antimony and silicon undergo a higher volume expansion than graphite and thereby generate large volume changes when used as electrode materials in lithium batteries [8–12]. This issue is the key obstacle to the commercial use of metal-based lithium-ion batteries. CNTs can potentially be used as active anode materials because of their high lithium insertion capacity [13–19], but their actual use is limited by their relatively poor lithium extraction capacity and their large irreversible capacities during repeated charging and discharging of lithium ions, so conventional graphite anode materials have been preferred. The incorporation of high-capacity lithium storage compounds such as tin nanoparticles into CNTs is expected to result in a high capacity and good cycleability. It is hoped that the use of CNT/tin nanoparticle composites can provide a solution to dimensional instability problems by limiting the changes in volume of electrodes.

For a CNT/tin nanoparticle composite to be used as an anode material, the tin nanoparticles have to be well-dispersed on the CNT network surfaces; the CNTs play an important role as conductive additives in the anode system because of the formation of a nano-sized conductive network linking the tin nanoparticles, and their high electronic conductivity and large surface area. Furthermore, the buffering effect of CNT/tin nanoparticle composites gives the batteries dimensional stability, which is important because the outer dimensions of batteries are strongly influenced by the expansion or shrinkage of electrode materials [20]. In other words, the presence of CNTs can prevent the repeated aggregation and pulverization of the dispersed tin nanoparticles during charging and discharging. In addition, both CNTs and tin nanoparticles are electrochemically active and can react with lithium ions, so they form composites without diminishing the specific capacity. The mechanisms of electrode operation during lithium insertion and extraction are shown in Fig. 4 for three different electrode materials, namely: a CNT electrode system (Fig. 1a), a tin nanoparticle-based electrode system (Fig. 1b), and an electrode system based on a CNT/tin nanoparticle composite (Fig. 1c). The development of high-dispersion methods for the fabrication of CNT/tin nanoparticle composites with highly stable cycle performance is essential for their practical application in rechargeable lithium-ion batteries.

Several different approaches have been used to fabricate CNT/tin and CNT/tin oxide composites. Mechanical mixing of CNT and metal nanoparticles [3] and chemical reduction of tin salts

* Corresponding author. Tel.: +82 42 350 3931; fax: +82 42 350 3910.
E-mail address: heetae@kaist.ac.kr (H.-T. Jung).

0378-7753/$ – see front matter © 2009 Elsevier B.V. All rights reserved.
doi:10.1016/j.jpowsour.2009.04.045

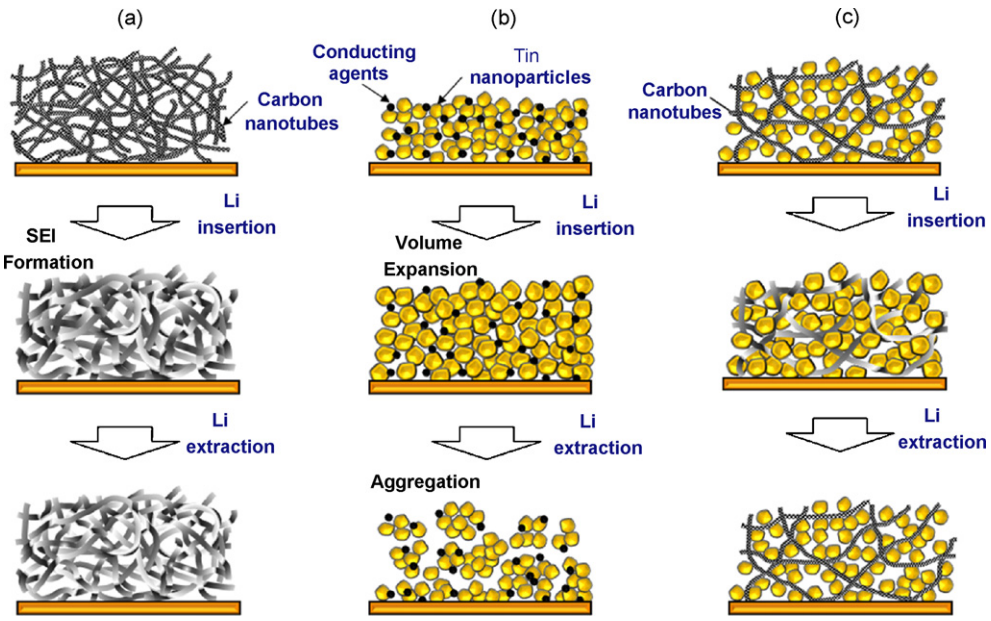

Fig. 1. (a) Mechanism of capacity fading in CNT electrodes, (b) aggregation of tin nanoparticles during lithium insertion and extraction cycling and (c) schematic representation of CNT/tin nanoparticle composite.

in CNT suspensions [4–6] have been used to fabricate CNT/tin nanoparticle composite electrode systems for application in lithium-ion batteries. The fabrication of tin-filled CNTs as insertion anode materials has been used to introduce tin salts into oxidatively opened nanotubes through capillary action, followed by the reduction of the tin salts [7]. The employment of block copolymer template composite electrodes for the fabrication of rechargeable lithium batteries has also been reported, with the preferred localization of the CNTs and metal salt in the polar blocks [21]. However, the applicability of CNT/tin nanoparticle composites as anode materials in rechargeable lithium batteries is limited by the difficulties with the above methods of obtaining a fine dispersion of tin nanoparticles in the CNTs and their inefficient processing conditions that result in critical reductions in the cycleability.

This study involves two new approaches to preparing well-dispersed, single-walled carbon nanotube (SWNT)/tin nanoparticle composite films on electrode substrates for use as anode electrodes: (i) a hybrid co-filtration method and (ii) a combined method composed of vacuum filtration and electrochemical reduction. It is found that the resulting hybrid composite films are very uniform, and that with these fabrication methods the tin nanoparticles are homogeneously trapped in the SWNT networks. The results with coin-cell type lithium secondary batteries show that their reversibility and power performance are greatly enhanced over prolonged cycling when compared with those of tin nanoparticle and SWNT electrodes.

2. Experimental

Commercialized SWNTs of carboxylic acid functionalized grade from Cheaptubes Inc., which have good dispersibility in N-methyl-2-pyrrolidone (NMP) and dimethyl formamide (DMF), were used in the experiments.

The SWNT/tin nanoparticle composites were prepared via two different methods (Fig. 2), namely: (i) electroplating of the tin nanoparticles by reduction of tin ions on to vacuum-filtered SWNT films (Fig. 2a) and (ii) a hybrid co-filtration method by vacuum filtration of SWNT/tin nanoparticle hybrid solutions (Fig. 2b). The electrochemical reduction of tin sulfate over the vacuum-filtered CNT networks was carried out by applying the appropriate voltage with the following procedure. First, pure CNT network films were prepared. 20 mg of CNTs were placed in 200 mL of DMF and homogenized with a horn-type ultrasonic processor with a power of 300 W in the pulse mode for 1 h. This CNT suspension was centrifuged for 1 h at 15 000 rpm. The supernatant was used to fabricate the network film and the sediment was collected and weighed after drying. CNT networked film electrodes were prepared by using the vacuum filtration method. A calculated amount of the above supernatant suspension was vacuum filtered by using a Whatman Anodisc47 alumina filter with 20 nm pores and an effective area of 11.3 cm^2. After vacuum filtration, the alumina filter loaded with CNTs was placed in a 3 mol L^{-1} NaOH solution, which was then repeatedly replaced with distilled water until the pH was about 7. A copper foil was positioned beneath the floating electrode and the electrode was then attached to the copper foil by draining the distilled water. After predrying at 60 °C, the electrode was washed with distilled water and dried at 60 °C again. Finally, the electrode was dried under vacuum at 120 °C, and purged with argon. The CNT electrode was used as a working electrode during electrodeposition by firmly clamping it under the electrolyte to prevent leakage of electrolyte (see the supplementary information, Fig. S1). The electrolyte

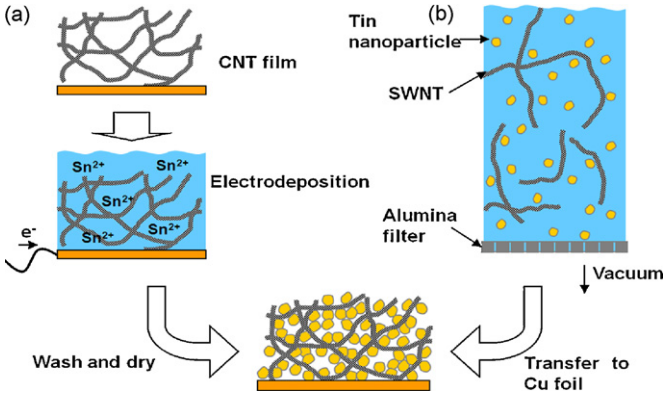

Fig. 2. Schematic representations of novel methods for preparing composites: (a) electroplating tin nanoparticles on to vacuum-filtered SWNT films and (b) hybrid co-filtration of SWNTs and tin nanoparticles.

consisted of 1 mol L^{-1} H_2SO_4 and 0.01 mol L^{-1} $SnSO_4$ aqueous solution [22,23]. The electroplating of tin nanoparticles was performed by using the chronoamperometry technique at a constant potential (−0.45 V vs. a standard calomel electrode, as determined with linear sweep voltammetry; see the supplementary information, Fig. S2). The quantity of electroplated tin nanoparticles was controlled by varying the time of reaction. The composite electrodes having SWNT:tin weight ratio of 1:1 and 1:2 were prepared by this method.

The other method used in the preparation of the SWNT/tin nanoparticle composites was hybrid co-filtration (see Fig. 2b). This method results in only physical contact between the CNTs and the tin nanoparticles, but it is easy to apply and can be used to manufacture electrodes with a higher loading of active materials. The tin nanoparticles were purchased from Aldrich, and the average particle size was found to be 100 nm. A predetermined ratio of the tin nanoparticles and the SWNTs was dispersed in DMF and sonicated. This mixed suspension was filtered under vacuum with the same method as described above for the CNT networks, and then transferred on to the copper foil. A composite electrode with a SWNT:tin weight ratio of 1:9 was prepared by this method.

The electrochemical characterizations were carried out with coin cells. Type 2016 coin cells (20 mm diameter and 1.6 mm thickness) were prepared using the above electrodes, porous polyethylene separators, lithium metal foil, Ni foam, and an electrolyte. The nonaqueous electrolyte was composed of 1 mol L^{-1} LiPF6, ethylene carbonate (EC) and diethyl carbonate (DEC) at 33 and 67 vol.%, respectively, and 3 wt.% of vinyl carbonate (VC) as an additive. The cells were assembled in an argon-filled glove box.

Both charging and discharging were carried out galvanostatically at a current density of 0.05C in the first cycle, and at 0.2 or 0.5C in subsequent cycles. The charging and discharging were potential controlled with a cut-off of 0 V vs. Li/Li^+ for lithium insertion and 2 V vs. Li/Li^+ for lithium extraction. All the charging and discharging tests were carried out with a battery tester manufactured by Toyo System (TOSCAT 3100).

3. Results and discussion

The methods for the fabrication of CNT/tin nanoparticle composite films on the electrode substrates are illustrated schematically in Fig. 2. SWNTs were used as the framework materials because it is commonly accepted that SWNTs have larger lithium insertion ability than multi-walled carbon nanotubes (MWNTs) due to their better conductive connecting ability, which arises from their higher specific surface area and larger aspect ratio [24].

In the electroplating method (Fig. 2a), highly uniform SWNT network films were prepared on copper substrates using the vacuum filtration method [25–27] (see Fig. 3a). The SWNT film specimens were then immersed in a tin salt solution for various amounts of time to attach tin nanoparticles to the SWNT network films. The electroplating reaction potential was determined to be −0.45 V vs. the reference electrode (saturated calomel electrode, SCE) with linear sweep voltammetry (see the supplementary information). The electroplating of tin nanoparticles on to the SWNT electrodes was then performed at a constant potential with respect to the reference electrode by using the chronoamperometry technique. A scanning electron microscope (SEM) image shows that highly uniform tin nanoparticles with sizes in the range 10–30 nm cover the SWNT network surfaces (Fig. 3b). The amount and size of the tin nanoparticles are controlled by varying the duration of the electrochemical reduction of the tin ions. In the hybrid co-filtration method (Fig. 2b), simultaneous vacuum filtration was carried out with SWNT/tin hybrid solutions. SWNT/tin hybrid solutions with various mass ratios and concentrations were prepared by mixing prepared tin nanoparticle and SWNT suspensions; the tin nanoparticle (or SWNT) suspensions were obtained by dispersing the tin (or carboxylic acid functionalized SWNTs) in NMP or DMF with the aid of an ultrasonic processor. After vacuum filtration, each composite film was transferred to the copper substrate, and then used as a lithium-ion battery electrode. In the case of electroplated SWNT/tin nanoparticle composites (Fig. 3b), the SWNT/tin nanoparticle composite films prepared from vacuum-filtered composites are found to contain a fine dispersion of tin nanoparticles with SWNTs on the electrode substrates, which arises because tin nanoparticles are captured in the CNT networks during vacuum filtration (Fig. 3c). Thus, the SWNT networks retain the tin nanoparticles mechanically and electronically. These two composite electrode fabrication methods are found to deliver anodes with very similar electrochemical performance in lithium-ion batteries, but the hybrid co-filtration method is more suitable for higher SWNT:tin ratios.

Fig. 4 shows the cycle-life performance at an electrode density of 5 mg cm^{-2} of three different battery anode electrodes, namely: a SWNT film electrode (triangles), a tin nanoparticle electrode (squares), and a SWNT/tin nanoparticle composite electrode with a weight ratio of 1:9 (circles). The electrochemical measurements were performed using coin-type lithium-ion half-cells. All three electrodes exhibit small losses during the first few cycles, but their stabilities and capacities during cycling are very different. The specific capacities of the tin nanoparticle electrode (see the leftmost square in Fig. 4a; 702 mAh g^{-1}) and the SWNT/tin nanoparticle composite electrode (see the leftmost sphere in Fig. 4a; 672 mAh g^{-1}) are much higher than that of the SWNT electrode (see the leftmost triangle point in Fig. 4a; 334 mAh g^{-1}), due to the intrinsic high specific capacity of lithium–tin alloy formation. More importantly, it is found that the capacity retention of the composite electrode improves significantly during prolonged cycling, unlike that of either the SWNT or the tin nanoparticle electrode. The SWNT/tin nanoparticle composite electrode exhibits a high specific capacity of ∼500 mAh g^{-1} for up to fifty cycles with a relatively stable performance, whereas there is an abrupt capacity fading

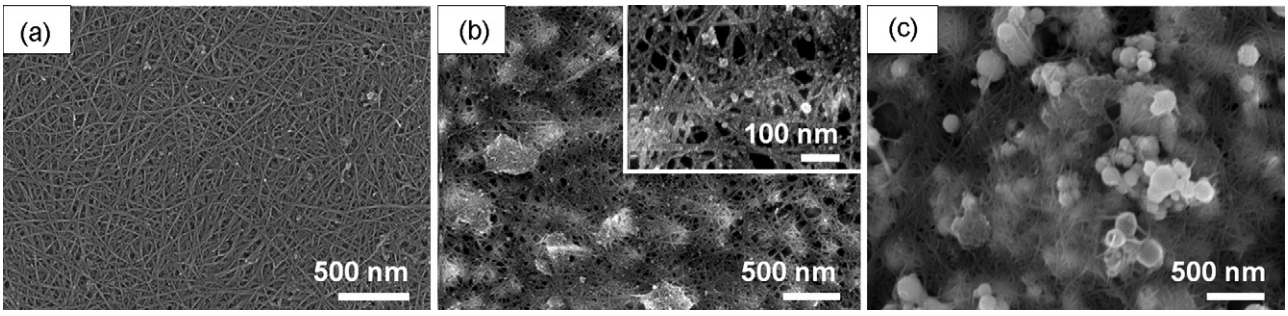

Fig. 3. SEM images of (a) vacuum-filtered CNT network film, (b) tin nanoparticle electroplated CNT electrode and (c) SWNT/tin nanoparticle composite prepared by hybrid co-filtration.

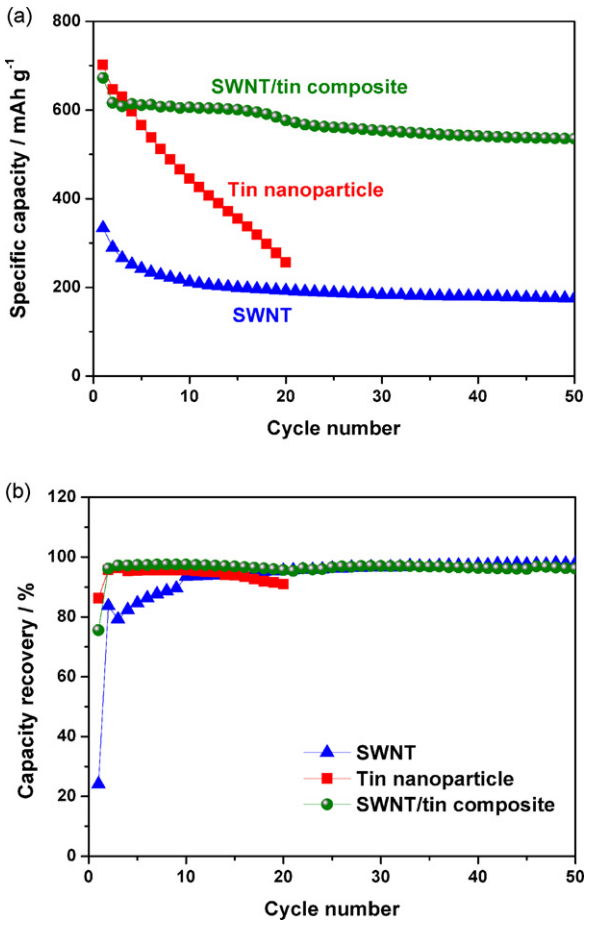

Fig. 4. (a) Variation of reversible specific capacities of electrodes with number of cycles and (b) variation of charge recovery of electrodes with number of cycles. Current density is 0.2C and electrode density is 5 mg cm^{-2}.

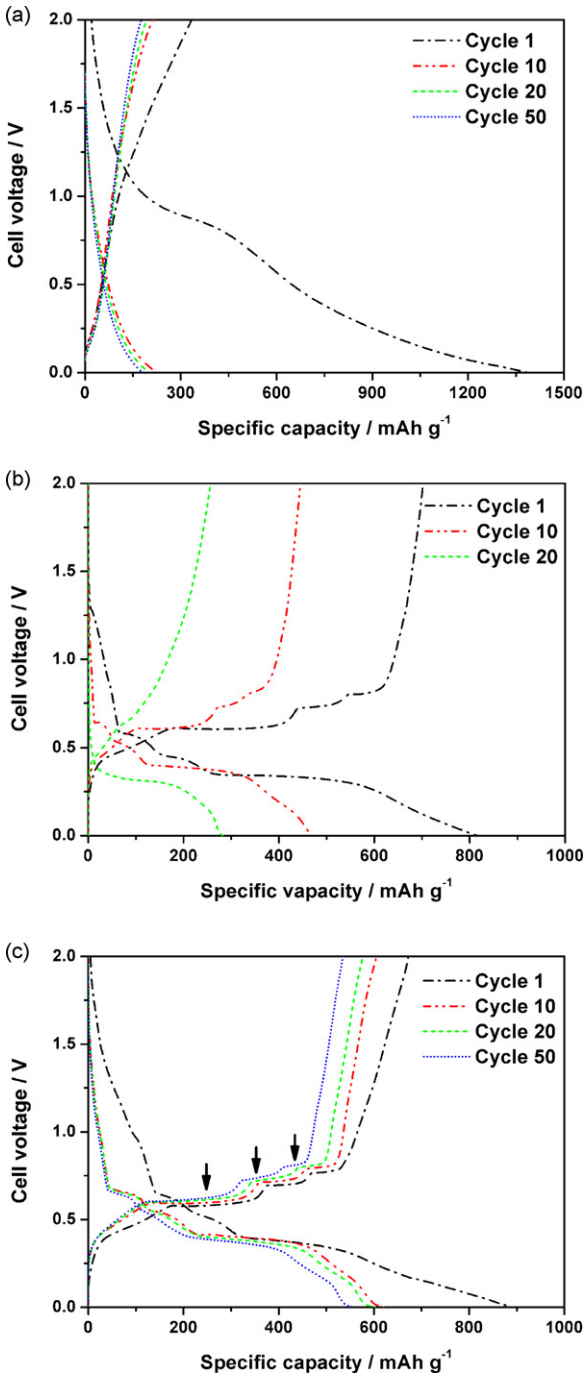

Fig. 5. Voltage profiles of coin-type lithium rechargeable batteries during cycling at selected cycle numbers: (a) SWNT electrode, (b) tin nanoparticle electrode and (c) SWNT/tin nanoparticle composite electrode.

for the tin nanoparticle and SWNT electrodes after three cycles. Note that even though the weight ratio of CNTs is only 10%, the composite electrode displays acceptable cycleability. The specific capacity of the composite electrode increases with increase in the weight ratio of tin nanoparticles, e.g., 410 mAh g^{-1} for a composite weight ratio of 1:1, 520 mAh g^{-1} for a composite weight ratio of 1:2, and 672 mAh g^{-1} for a composite weight ratio of 1:9 (data not shown). The additional advantage of increasing the proportion of tin nanoparticles in the composite is the reduction in irreversible reactions during the first cycle. The reversibility or charge recovery of the SWNT electrode is only 24.1% (see the leftmost triangle in Fig. 4b), and that of the tin nanoparticle electrode is 86.2% (see the leftmost square in Fig. 4b). The charge recovery of the composite electrode is close to that of the tin nanoparticle electrode (see the leftmost square in Fig. 4b; 75.6%). High electrode reversibility is very important for practical battery applications. The uniformity and homogeneity of the composite make it possible to lower the CNT weight ratio and retain good cycleability. By contrast, fabrication by chemical reduction of the tin salt in CNT aqueous suspension results in CNT bundle formation or aggregation, so more CNTs are required. The use of SWNTs rather than MWNTs also enables the use of a lower weight ratio of CNTs because of their higher aspect ratio. These coulombic efficiency (charge recovery) and cycle-life performance results are better than those obtained with other composite fabrication methods.

The SWNT electrode exhibits a large specific charge capacity during the first cycle (1 388 mAh g^{-1}) (see Fig. 5a) which is almost four times higher than that of graphite, which has a theoretical capacity of 375 mAh g^{-1}, and a typical capacity of 330 mAh g^{-1}. In the other hand, the specific discharge capacity (334 mAh g^{-1}) at the first cycle is significantly lower than the charge capacity (1 388 mAh g^{-1}), with a reversibility of 24.1%. The low reversibility and capacity fading during the first three cycles are due to the large surface area of the SWNTs. The specific capacity stabilizes at ~200 mAh g^{-1} after five cycles. The tin nanoparticle electrode has a higher specific capacity than the graphite and SWNT electrodes, but its discharging capacity decreases continuously with increase in cycle number (squares of Figs. 4a and 5b). This capacity fading might be due to repeated nanoparticle aggregation and pulverization during cycling. Nano-sized particles aggregate eas-

ily, and volume changes during repeated charging and discharging could accelerate this agglomeration. By contrast, the SWNT/tin nanoparticle composite electrodes prepared with the hybrid co-filtration method or electroplating plus vacuum filtration method have significantly enhanced cycle-life characteristics (see squares of Figs. 4a and 5c). The capacity retention of the 50th cycle is 87% with respect to the second cycle, and 80% with respect to the first cycle. This enhancement is due to the increased opportunity for contact between the SWNTs network and the tin nanoparticles, and they maintain this interfacial contact during prolonged cycling. Even though the CNT content of the composites is only 10 wt.%, they act as conducting wires and buffer materials for stress release. The specific capacity decreases slightly during the first two cycles due to the irreversible surface reactions of the SWNTs, and the capacity remains almost constant up to 50 cycles.

The potential profiles of the three different electrodes during charge–discharge cycles in the constant current mode (approximately 0.2C; 140 mA g^{-1} for the tin nanoparticle electrode and the CNT/tin nanoparticle composite electrode, 70 mA g^{-1} for the SWNT electrode) are shown in Fig. 5. The voltage profile of the composite electrode remains almost constant during cycling (Fig. 5c), whereas the specific capacity of the tin nanoparticle electrode decreases and its voltage profile goes through a broad transition (Fig. 5b). Three potential plateaux are observed for the composite electrode (indicated by arrows) during cycling, and correspond to the formation of Li_2Sn_5, LiSn, and Li_7Sn_3 phases [28]. This observation indicates that the tin nanoparticles maintain their good dispersion in the SWNT networks during prolonged cycling. In the case of the tin nanoparticle electrode (Fig. 5b), however, the plateaux start to disappear after 10 cycles, indicating the aggregation of the nanoparticles during the lithium alloying and dealloying processes.

To examine further the oxidation and reduction reactions during cycling, the differential capacity of each electrode was measured. There is significant formation of a solid electrolyte interphase (SEI) film on the SWNT electrode at 0.8 V (see filled circles in Fig. 6a) owing to the large specific surface area of the SWNTs, and the lithium-ion intercalation reaction occurs on the SWNT electrode at 0.1 V (see filled squares in Fig. 6a). Examination of the reaction peaks for the tin nanoparticle electrode, discloses distinctive lithium alloying reactions (see filled triangles in Fig. 6a) and lithium dealloying reactions (see filled reverse triangles in Fig. 6a). In the case of the SWNT/tin nanoparticle composite electrode, the mixed reduction of SWNTs and tin nanoparticles occurs during the first cycle. The SEI film formation on the surfaces of the SWNTs in the composite electrode (see open circles in Fig. 6a) and the lithium-ion intercalation reaction (see open squares in Fig. 6a) occur at the same voltage as the SWNT electrode. Moreover, alloying (see open triangles in Fig. 6a) and dealloying (see open reverse triangles in Fig. 6a) reactions occur between lithium and tin in the SWNT/tin nanoparticle composite electrode, and these reactions are also found in the tin nanoparticle electrode. Although the CNTs and tin nanoparticles are present in a composite, they react with lithium ions independently, and thus characteristic reaction peaks are present in the differential capacity curves. These alloying and dealloying reactions remain constant for up to 50 cycles, indicating that the tin nanoparticles in the hybrid composites do not aggregate during cycling (Fig. 6b). The SEI formation reaction does not occur in later cycles, whereas the lithium intercalation reaction of the SWNTs occurs continuously up to the 50th cycle. This means that the SWNTs act not only as an electrical and mechanical network but also as a host material for lithium ions and thus increase the specific capacity.

To investigate the effect of varying the electrode density on the cycle performance, hybrid composite electrodes with three different electrode densities, namely, 0.1, 0.5 and 5 mg cm^{-2} were tested (Fig. 7a). This range of electrode densities covers those of thin-film batteries (~0.1 mg cm^{-2}) and commercialized lithium-ion batteries (~5 mg cm^{-2}). The specific capacity decreases with increasing electrode loading, possibly because of the variation in the electrical contact between the SWNTs and the tin nanoparticles with electrode density. It is likely that most of the tin nanoparticles are in strong contact with the SWNTs in the thin electrode with a relatively low electrode density (0.1 mg cm^{-2}). As the electrode films become thicker, decrease in the opportunity for contact between the SWNTs and tin nanoparticles result in slight decreases in the specific capacity. Nevertheless, the cycle performance of these three electrodes is similar and thereby suggests that the proposed composite preparation method can be applied to a wide range of electrode densities.

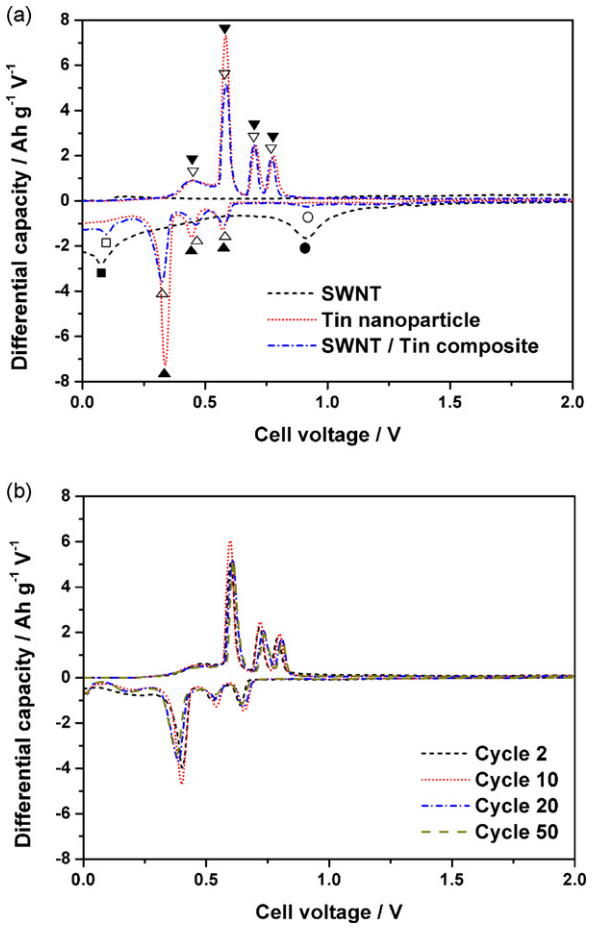

Fig. 6. (a) Differential capacity curves of three different electrodes at initial charge and discharge. (b) Differential capacity curves of SWNT/tin nanoparticle composite electrode at second, tenth, twentieth, and fiftieth cycles.

The well-dispersed nanoscale composites have good rate capability. Fig. 7b shows the cycle performance during charging and discharging for two current densities of 0.2C (0.7 mA cm^{-2}) and 0.5C (1.75 mA cm^{-2}), which is a requirement for commercialized batteries. Most prior research into the battery applications of these materials have been performed at a current density of 0.05C, which is inadequate for testing the high-current driven degradation of practical electrode systems. The cycleabilities of the SWNT/tin nanoparticle composite electrode at these two different current densities are quite similar, indicating that they have high power characteristics. Higher power performance is usually obtained when the size of the active material is small, and when the electronic conductance of the overall electrode is high [29,30]. Thus the two requirements for high power performance can be fulfilled in these homogeneous composites.

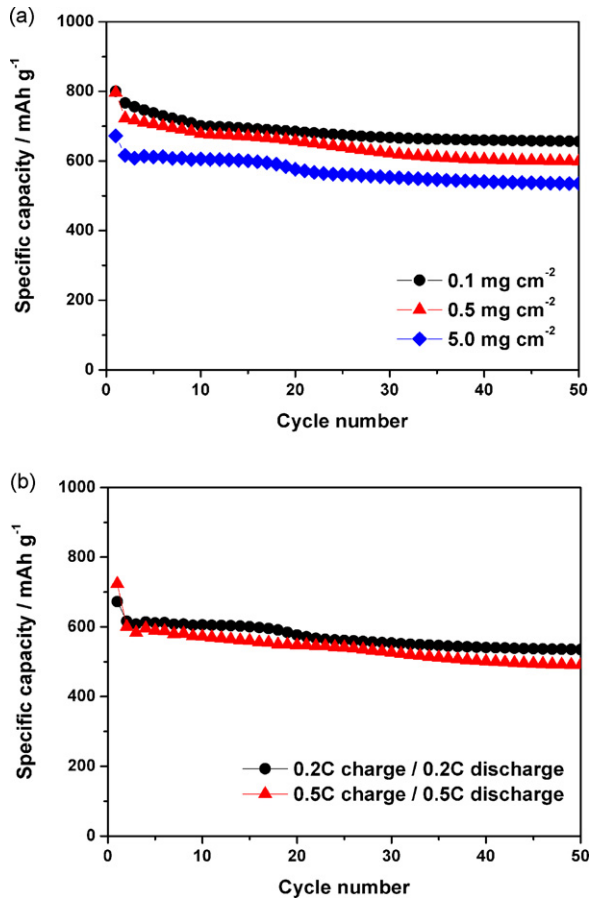

Fig. 7. (a) Specific capacities of various electrode densities with number of cycles at current density of 0.2C in all cases. (b) Specific capacities of vacuum-filtered composite electrode with an electrode density of 5 mg cm^{-2} versus cycle numbers with two different charge/discharge rates.

4. Conclusions

The techniques of hybrid co-filtration and the electrochemical reduction of tin ions combined with vacuum filtration of SWNTs for the fabrication of SWNT/tin nanoparticle composites on electrode substrates provide a fine dispersion of tin nanoparticles on SWNT network films. The cycle performance of the composites are found to be significantly better than those of SWNT/tin nanoparticle composite electrode films obtained with previous methods. Their electrical contacts are maintained during lithium insertion and extraction on cycling, and their morphology is not disrupted. The fabrication method is also potentially applicable to devices requiring the homogeneous dispersion of metal nanoparticles on CNTs, such as supercapacitor electrodes, fuel cell electrodes, chemical sensors, and dye-sensitized solar cells.

Acknowledgements

The work was supported by the National Research Laboratory Program of the Korea Science and Engineering Foundation (KOSEF), the Center for Nanoscale Mechatronics and Manufacturing (CNMM) and CUPS-ERC.

Appendix A. Supplementary data

Supplementary data associated with this article can be found, in the online version, at doi:10.1016/j.jpowsour.2009.04.045.

References

[1] W.-Q. Han, A. Zettl, Nano Lett. 3 (2003) 681–683.
[2] Z. Wang, G. Chen, D. Xia, J. Power Sources 184 (2008) 432–436.
[3] J.Y. Eom, J.W. Park, H.S. Kwon, S. Rajendran, J. Electrochem. Soc. 153 (2006) A1678–A1684.
[4] Z. Wen, Q. Wang, Q. Zhang, J. Li, Adv. Funct. Mater. 17 (2007) 2772–2778.
[5] M.-S. Park, S.A. Needham, G.-X. Wang, Y.-M. Kang, J.-S. Park, S.-X. Dou, H.-K. Liu, Chem. Mater. 19 (2007) 2406–2410.
[6] Z.P. Guo, Z.W. Zhao, H.K. Liu, S.X. Dou, Carbon 43 (2005) 1392–1399.
[7] T.P. Kumar, R. Ramesh, Y.Y. Lin, G.T. Fey, Electrochem. Commun. 6 (2004) 520–525.
[8] H. Lee, J. Cho, Nano Lett. 7 (2007) 2638–2641.
[9] Y. Yu, C.-H. Chen, Y. Shi, Adv. Mater. 19 (2007) 993–997.
[10] L. Simonin, U. Lafont, E.M. Kelder, J. Power Sources 180 (2008) 859–863.
[11] M. Marcinek, L.J. Hardwick, T.J. Richardson, R. Kostecki, J. Power Sources 173 (2007) 965–971.
[12] J.-M. Tarascon, M. Armand, Nature 414 (2001) 359–367.
[13] G. Che, B.B. Lakshmi, E.R. Fisher, C.R. Martin, Nature 393 (1998) 346–349.
[14] R.S. Morris, B.G. Dixon, T. Gennett, R. Raffaelle, M.J. Heben, J. Power Sources 138 (2004) 277–280.
[15] Y.A. Kim, M. Kojima, H. Muramatsu, S. Umemoto, T. Watanabe, K. Yoshida, K. Sato, T. Ikeda, T. Hayashi, M. Endo, M. Terrones, M.S. Dresselhaus, Small 2 (2006) 667–676.
[16] M. Baibarac, M. Lira-Cantu, J. Oro-Sole, N. Casan-Pastor, P. Gomez-Romero, Small 2 (2006) 1075–1082.
[17] X.X. Wang, J.N. Wang, H. Chang, Y.F. Zhang, Adv. Funct. Mater. 17 (2007) 3613–3618.
[18] A. Kiebele, G. Gruner, Appl. Phys. Lett. 91 (2007) 144104.
[19] A.S. Claye, J.E. Fischer, C.B. Huffman, A.G. Rinzler, R.E. Smalley, J. Electrochem. Soc. 147 (2000) 2845–2852.
[20] J.H. Lee, H.M. Lee, S. Ahn, J. Power Sources 119–121 (2003) 833–837.
[21] S.C. Mui, P.E. Trapa, B. Huang, P.P. Soo, M.I. Lozow, T.C. Wang, R.E. Cohen, A.N. Mansour, S. Mukerjee, A.M. Mayes, D.R. Sadoway, J. Electrochem. Soc. 149 (2002) A1610–A1615.
[22] W. Wang, P.N. Kumta, J. Power Sources 172 (2007) 650–658.
[23] E. Gomez, E. Guaus, F. Sanz, E. Valles, J. Electroanal. Chem. 465 (1999) 63–71.
[24] T.M. Day, P.R. Unwin, N.R. Wilson, J.V. Macpherson, J. Am. Chem. Soc. 127 (2005) 10639–10647.
[25] N.P. Armitage, J.-C.P. Gabriel, G. Gruner, J. Appl. Phys. 95 (2004) 3228–3230.
[26] Z. Wu, Z. Chen, Z. Du, J.M. Logan, J. Sippel, M. Nikolou, K. Kamaras, J.R. Reynolds, D.B. Tanner, A.F. Hebard, A.G. Rinzler, Science 305 (2004) 1273–1276.
[27] B.-S. Kong, D.-H. Jung, S.-K. Oh, C.-S. Han, H.-T. Jung, J. Phys. Chem. C 111 (2007) 8377–8382.
[28] T.B. Massalski, Binary Alloy Phase Diagrams, ASM international, Ohio, 1999, pp. 2469–2470.
[29] C.R. Sides, N. Li, C.J. Patrissi, B. Scrosati, C.R. Martin, MRS Bull. 27 (2002) 604–607.
[30] A.S. Arico, P. Bruce, B. Scrosati, J.-M. Tarascon, W.V. Schalkwijk, Nat. Mater. 4 (2005) 366–377.